Geochemical records in subaerial exposure environments in Croatia using discriminant function analysis of bauxite data

Nikolina Ilijanić*, Erli Kovačević Galović, Nikola Gizdavec,
Ivona Ivkić Filipović, Slobodan Miko* and Zoran Peh

Croatian Geological Survey, Zagreb, Croatia

Croatian bauxites are long known for their chemical and physical diversity arisen from their characteristic origin and emplacement within the area of the Adriatic−Dinaric carbonate platform (ADCP). They include eight horizons spanning the period between the Upper Triassic (Carnian) and the Miocene, formed on subaerially exposed platform paleoenvironments. The bauxite genesis is recorded in the bauxite geochemical composition as a unique signature of tectonostratigraphic evolution of the different parts of the Croatian Karst, including, for example, the forebulge unconformity typical for the Istrian area. In this work, an explanation of the typical patterns of bauxite formation is based on the construction of a discriminant function model (DFM) resulting from the compositional data (CoDa) analysis of bauxite geochemical data (major and trace elements). The model shows that the greatest part of the variation contained in the analyzed bauxite data (the first discriminant function, DF1) is associated with systematic alteration of geochemical composition in time, emphasizing characteristic decrease in clay component and gradual enrichment in heavy metals from oldest (Upper Triassic) to the youngest (Miocene) bauxites. In the general scheme, particular bauxite horizons represent standalone groups (Upper Triassic) while others form clusters showing increase and/or decrease of a particular set of elements signaling the changes in environmental conditions during the considered geological history of ADCP. Other discriminant functions (DF2 and DF3) also contribute to the all-inclusive distinction between the eight a priori defined bauxite groups discriminated by the characteristic set of geochemical variables where DF2 typically refers to the process of desilication, while DF3 to that of deferralitization.

Introduction

The karst bauxites are broadly recognized as regional markers of diverse largescale events impacting the carbonate platforms in particular periods of their geological history when warm and humid climates conjoined to their tectonically controlled subaerial exposure (D'Argenio and Mindszenty, 1992; Mindzenty et al., 1995). Thus, the karst bauxites in general, and those originated in the plate-interior settings such as the Croatian Karst Dinarides in particular, assume the typical geochemical signature that may help elucidate specific issues concerning their genesis. In Croatia, however, regardless of extensive bauxite research and mining activities during more than half a century that generated copious mineralogical and chemical records, the question of bauxite genesis, especially on the subject of paleokarst and its tectonostratigraphic constraints, has been greatly unappreciated. Most probably, this disadvantageous position resulted from former predominant perceptions of bauxites as predominantly an aluminum ore, focusing all research efforts on the appraisal of aspects concerning their finding, exploitation and refinement. Sometimes, they were considered in broader perspective of local tectonics (Blašković et al., 1989), as well as paleoclimate related mineralogical and geochemical processes (e.g., Šinkovec and Sakač, 1982; 1991; Sakač and Šinkovec, 1991) but their tectonically instigated origin was brought to a focus only after the construction of new models of orogenic evolution of the Adriatic (Adriatic/Dinaric) Carbonate Platform (ADCP). The latter referred specifically to the External Dinarides of the NE Adriatic region (Vlahović et al., 2005; Korbar, 2009; Brlek et al., 2014) taking also into account new ideas of "forebulge related unconformities associated with early stages of foreland basin development" (Crampton and Allen, 1995) that emphasized the importance of manifold stratigraphic gaps appearing in the Mesozoic-Tertiary successions of the Croatian Dinarides, as well as new insights into a potential source of the parent material (Merino and Banerjee, 2008; Šušteršič et al., 2009; Banerjee and Merino, 2011). That said, the complex investigation of bauxites as "tectonic and climatic event markers at regional unconformities" (D'Argenio and Mindszenty, 1995) became indispensable in search for a new lithostratigraphic scheme, setting the foundation for the regional correlation studies over the whole platform.
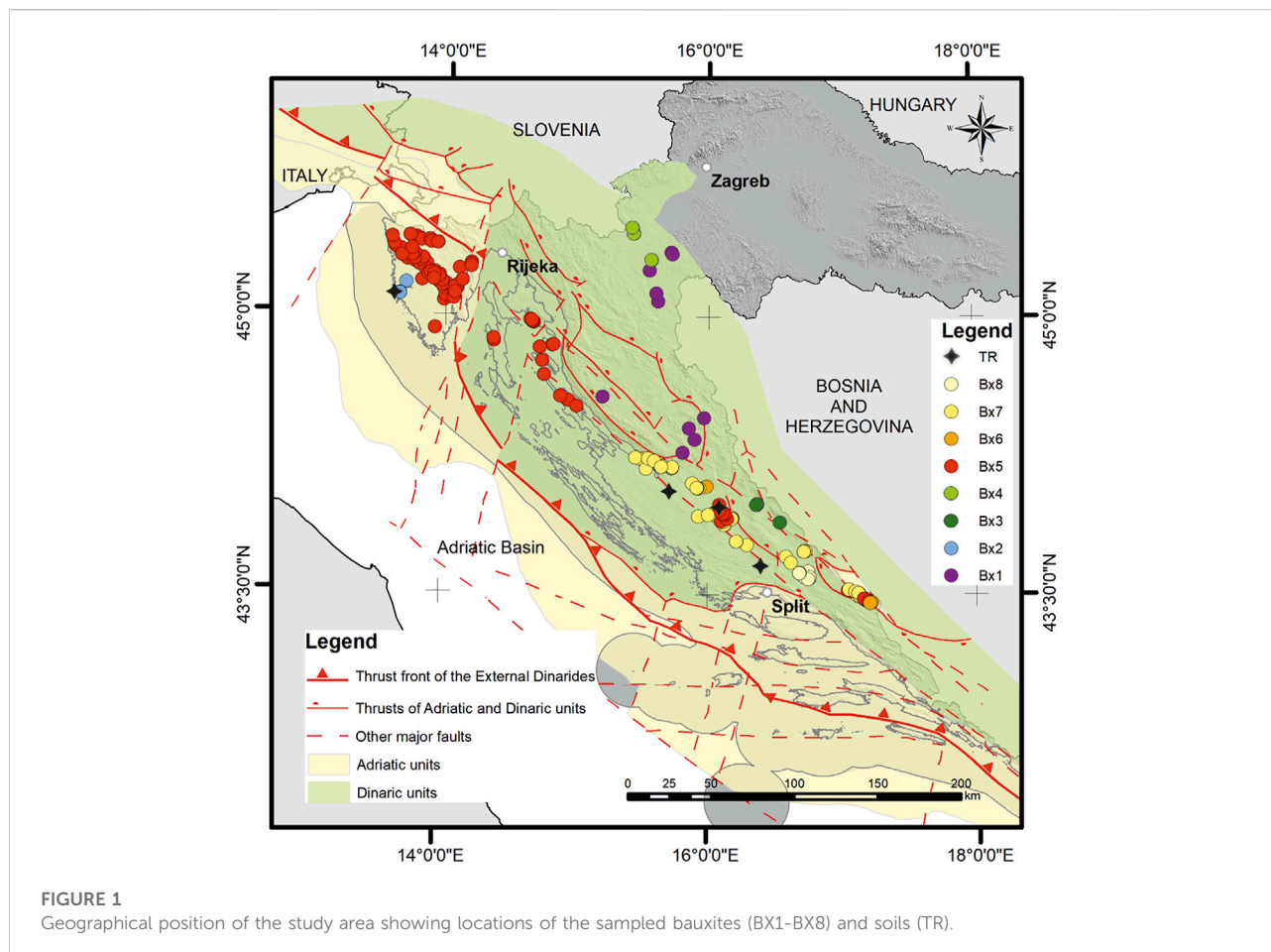
The basic premises of the recent investigations of bauxites in Croatia converged on geochemical variations detected in the bauxite deposits of the Lower Paleogene age (LPB) from the Croatian karst (Kovačević Galović et al., 2012). They employed statistical tools (discriminant function analysis), with special reference to the Istrian Peninsula because of its distinct geodynamic evolution through Cretaceous to Paleogene times (Peh and Kovačević Galović, 2014) and its relations to the rest of the ADCP in light of the ergodic hypothesis (swapping spatial for temporal variability) *via* comparison between two statistical

(discriminant) models (Peh and Kovačević Galović, 2016). The latest study addressed the issues of the bauxite formation during the Miocene climatic optimum, based mostly on high-precision zircon geochronology (Brlek et al., 2021). The main idea behind the present work revolves around explication of the typical patterns of bauxite formation grounded in the development of discriminant function models based on the Compositional Data (CoDa) analysis of bauxite geochemical data. This method provides solid ground for the separation of the various *a priori* defined bauxite groups deposited in the changing, subaerially exposed, ADCP paleoenvironments from the earliest (Upper Triassic) to the latest (Miocene) periods of bauxite formation in accordance with their geochemical signature. In a sense, this study is a continuation of earlier investigations performed more locally with focus on the single (K/Pg) unconformity at the same platform (Kovačević Galović et al., 2012; Peh and Kovačević Galović 2014; Peh and Kovačević Galović 2016) which have been launched with the purpose of initiating the regional correlation studies within the entire area of the Croatian Karst Dinarides. This study presents a step further, trying to elucidate the patterns of bauxite formation through time as defined by eight successive regional unconformities ranging from Triassic to Neogene times.

The whole rock geochemical data analyzed here are of compositional nature (represented in wt% and mg/kg), providing information about relative magnitudes (as proportions of the whole). Thus, their statistical treatment is necessarily focused on the log-ratio approach introduced by Aitchison, 1982; Aitchison, 1986 and disseminated by contemporary proponents of compositional data analysis (e.g., Aitchison and Egozcue, 2005; Tolosana-Delgado et al., 2005; Buccianti et al., 2006; Reimann et al., 2012; Buccianti, 2013).

Geological setting

Croatian bauxites belong to the karst type typical for the Circum-Mediterranean region. They are emplaced in the carbonate succession of the Croatian Karst (External or Outer) Dinarides, in places more than 8,000 m thick, whose deposits have a stratigraphic range from the Middle Permian (or even Upper Carboniferous) to the Eocene (Vlahović et al., 2002). Evolution of the area of Karst Dinarides started on a spacious epeiric carbonate platform along the northern Gondwana margin with the deposition of siliciclastic material in the Carboniferous, mixed clastic-carbonate sediments in the Permian and carbonate and mixed siliciclastic-carbonate deposits during the Early Triassic. Intense tectonic activity in the Middle Triassic led to the separation of the Adria Microplate characterized by a locally significant volcanoclastic input in the thick sequence of shallow-water carbonates. The Middle/Late Triassic boundary is marked mainly by a relatively long emersion phase with common bauxite occurrences, followed by the formation of the Southern Tethyan Megaplatform (Vlahović et al., 2005), a huge isolated

FIGURE 1
Geographical position of the study area showing locations of the sampled bauxites (BX1–BX8) and soils (TR).

intraoceanic platform represented by shallow-water carbonate deposits such as the Late Triassic Hauptdolomite and the Dachstein limestone. Segmentation of the huge platform into smaller carbonate platforms took place in the Late Lias resulting with the formation of the Adriatic Basin, with the Adriatic Carbonate Platform along its eastern side. Unresolved issues concerning the development of the Karst Dinarides at this stage of its development still remain (Vlahović et al., 2005, and references therein; Korbar, 2009, and references therein). Disagreements are exposed in different models of paleogeography and tectonostratigraphic constraints, particularly concerning Upper Cretaceous to Paleogene carbonates. The models in question assume the existence of a single (e.g., Vlahović et al., 2005), in contrast with the two carbonate platforms (e.g., Korbar, 2009) of characteristic two-domain Adriatic-Dinaric labelling (ADCP), each with different tectonostratigraphic constraints, that originated from disintegration of the Adriatic microplate (Adria) during the Upper Triassic—Lower Jurassic times and in later events at its plate boundaries (e.g., Vlahović et al., 2005; Schmid et al., 2008; Schmid et al., 2020; Korbar, 2009; Sisciani and Calamita, 2009; Márton, et al., 2010; Ustaszewski et al., 2010; Šumanovac, 2010;

Márton, et al., 2011; Nocquet, 2012; Hinsbergen et al., 2014). The first ("Dinaric") includes the recent External Dinarides region, a highly deformed fold-and-thrust belt of Alpine origins created by the collision of Adria with the Austroalpine and Tisia domains while the second ("Adriatic") represents the Adriatic foreland, a more stable portion of Adria distinguished by normal faults and gentle compressional late-orogenic deformations, both studded with numerous bauxite deposits (Figure 1).

Gradual subsidence of the platform basement in the Late Jurassic and Cretaceous enabled a profuse production of predominantly shallow-marine carbonates. However, the interaction of eustatic sea-level changes and synsedimentary tectonics resulted in frequent local or regional emersions of variable duration characterized by the deposition of bauxites. In the Late Cretaceous, a gradual disintegration of the platform started as a result of collisional processes, causing differentiation of sedimentary environments and culminating with the formation of flysch basins. At the transition from the Cretaceous to the Paleogene a general emersion of variable duration took place on the ADCP and the Paleogene transgression occurred mostly during the Eocene (Vlahović et al., 2005). Renewed carbonate sedimentation in the

Palaeogene was largely controlled by intense tectonics with carbonate deposition continuing on carbonate ramps while areas of primary carbonate production were increasingly overwhelmed by clastic deposition (Vlahović et al., 2002). Lower Paleogene Liburnian formation (including the Kozina beds) and Eocene foraminiferal limestones are followed by transitional beds and flysch (Korbar, 2009). Tectonic contraction of the platform area in the Oligocene-Miocene resulted in the uplift and formation of the present Dinarides (Vlahović et al., 2002).

Bauxites

Karst bauxites in Europe, both those formed in the plate-interior settings such as bauxites in Croatia (Karst Dinarides), Italy (Southern Apennines), Hungary (Villány region) and Greece (Parnassus, Ghiona and Helicon mountains), as well as those developed in plate-margin environments including Hungarian bauxites (Transdanubian Central Range), are thoroughly discussed in numerous works (e.g., Bardossy, 1982; Mindszenty et al., 1995; Mindszenty et al., 2000; Mondillo et al., 2011; Sakač and Šinkovec, 1991; Šinkovec and Sakač, 1982; and others). More recently, the emphasis is put on geochemical and mineralogical issues concerning parental affinities, weathering processes as well as climatic and tectonostratigraphic constraints during bauxite formation either in single deposits or in regional settings focused more often on a specific bauxite-bearing horizon (e.g. Mondillo et al., 2022; Abedini et al., 2018; Abedini and Khosravi, 2020; Boni et al., 2012; Boni et al., 2013; Brlek et al., 2021; Kelemen et al., 2022; Mongelli et al., 2014; Mongelli, 2002; Peh and Kovačević Galović 2014; Peh and Kovačević Galović 2016; Putzolu et al., 2018; Sinisi, 2018; Zhao et al., 2021; and others). Lately, bauxite research has particularly focused on the potential for REE and associated critical metals (e.g. Radusinović et al., 2016; Papadopoulos et al., 2019; Radusinović and Papadopoulos, 2021; Mondillo et al., 2019; Mongelli et al., 2017; Tomašić et al., 2021; Yang et al., 2019; and others). Widely identified as regional markers of global events, bauxites occurred in distinctive periods in the geological history with warm and humid climates conjoined with tectonically controlled subaerial exposure of the carbonate platform (D'Argenio and Mindszenty, 1992; D'Argenio and Mindszenty, 1995). As a result, the karst bauxites exhibit unique geochemical signature that may help explain specific issues with regard to their genesis. Both a general consent and wide disagreement occur in the geological community, firstly regarding their polygenetic nature—inferring karstification prior to deposition and transformation of the soil-derived proto-bauxitic material (terra rossa) (Durn et al., 1999; Durn et al., 2007)—and, secondly, concerning the ultimate source of the precursor material for the incipient bauxite-type soils. Dispute about their residual or detrital origin was recently given the new impetus by virtue of the novel conception of isovolumetric interaction between the carbonate
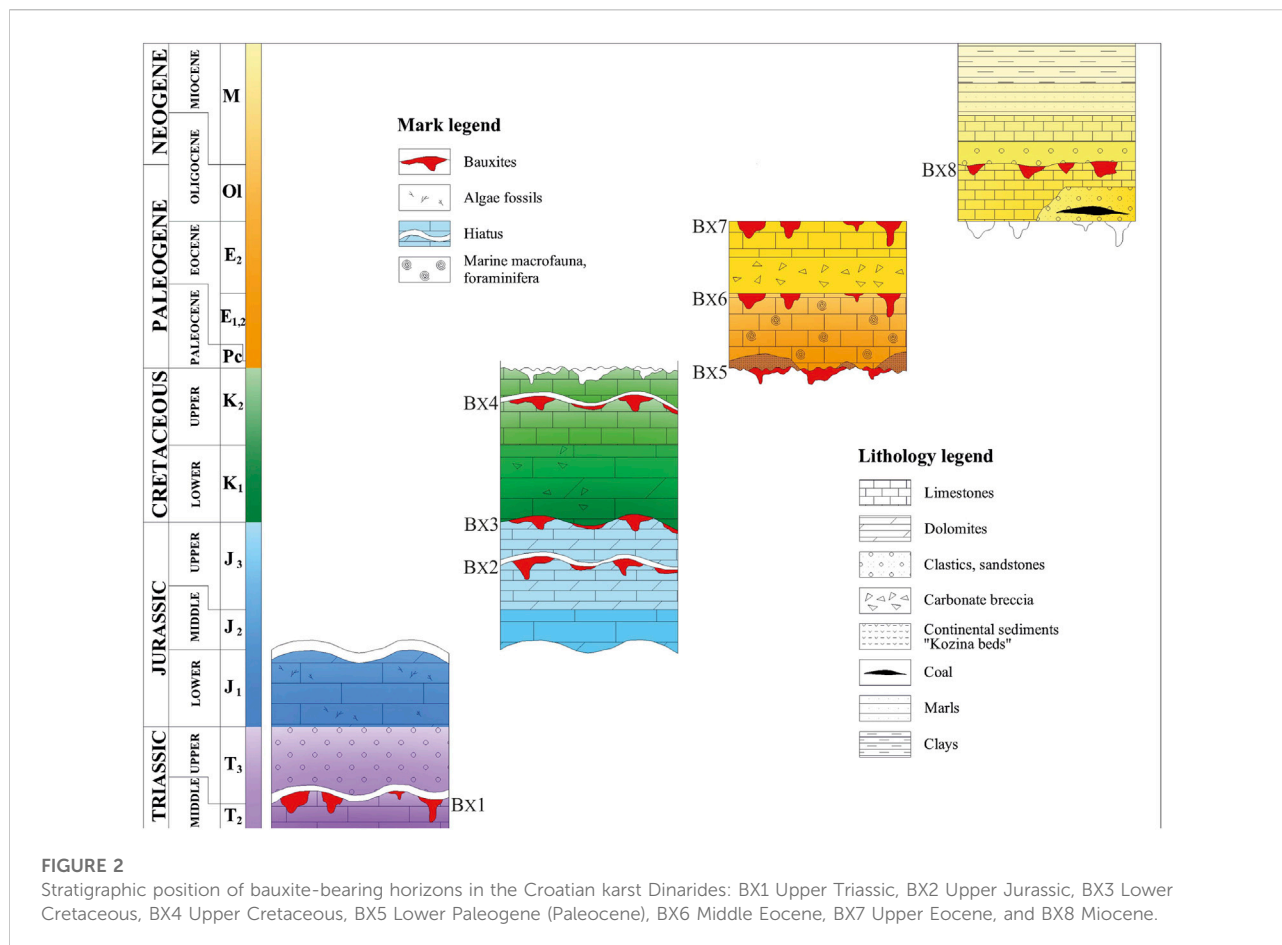
bedrock and airborne material (aeolian dust and volcanic ash), advanced by Merino and Banerjee (2008) and later expanded by Banerjee and Merino (2011). In this light the process of calcite substitution by clay prompts the origin of authigenic red claystone which subsequently undergoes pedogenesis. Combining the terra rossa as the proto-bauxitic material with processes of karst weathering occurring at its base presents the major paradigm shift in the genesis of karst bauxites. In this pattern the bauxite parent material is treated as paleosol derived from the interaction between the carbonate rock and airborne siliciclastic material—eolian and/or volcanic dust—or even terrestrial material such as loess or flysch (Durn et al., 1999; Durn 2003), as well as possible detritus from the neighboring ophiolitic complex replacing the older, residual, for new, detrital theory of bauxite origin.

Bauxites occur in various stratigraphic positions in the Croatian karst region, from the Triassic to the Miocene, with fundamental differences in chemical composition, mode of occurrence, and deposit type (Sakač and Šinkovec, 1991). According to their defined stratigraphic relationship to the basement and cover layers as well as the specific geotectonic position of a broad geographic scope, eight stratigraphic horizons of bauxite deposits were previously determined (Šinkovec and Sakač, 1991) (Figure 2) and are used in this study: 1) Upper Triassic (Carnian, BX1), 2) Upper Jurassic (Malmian, BX2), 3) Lower Cretaceous (Valanginian-Hauterivian, BX3), 4) Upper Cretaceous (Senonian, BX4), 5) Lower Paleogene (Paleocene, BX5), 6) Middle Eocene (BX6), 7) Upper Eocene (BX7), and 8) Miocene (BX8) (Figures 3A–E).

Materials and methods

Sampling, sample preparation and chemical analysis

Sampling was carefully designed to include the entire study area, comprising all investigated bauxite horizons bounded by regional unconformities, and carried out during several campaigns. A total of 219 samples (215 bauxite + 4 terra rossa samples) were collected at various sites from 8 previously determined bauxite horizons in the Croatian part of the ADCP. A single sample represents each site following the idea that bauxites from any single regional unconformity (from the Upper Triassic to the Miocene) should represent a bulk geochemical composition regardless of their particular positions within the ore body (e.g., at the contact with the related paleokarst or with its immediate cover), i.e., a composite sample. Following the results of previous investigations focused primarily on LPBs, it is tacitly accepted in the present work that multivariate analysis carried out on the bulk geochemistry of a number of cases is capable of identifying the most important geochemical processes addressing the bauxite autochthony-allochthony issues as well as those concerning vadose-phreatic depositional-diagenetic environments (D'Argenio and

FIGURE 2
Stratigraphic position of bauxite-bearing horizons in the Croatian karst Dinarides: BX1 Upper Triassic, BX2 Upper Jurassic, BX3 Lower Cretaceous, BX4 Upper Cretaceous, BX5 Lower Paleogene (Paleocene), BX6 Middle Eocene, BX7 Upper Eocene, and BX8 Miocene.

Mindszenty, 1995; Bardossy, 1982) simply by reducing all details along the vertical profile to a few mathematical functions.

Bauxite samples weighing about 3 kg in total were crushed by hand, split into fractions by quartering, and finally ground in a tungsten carbide pestle mortar mill (Retsch Lab Equipment) and sieved to .063 mm (all work done in Croatian Geological Survey laboratories) in preparation for the analytical work. Chemical analysis was performed at the Bureau Veritas laboratory (former ACME Analytical Laboratories Ltd.) in Vancouver, Canada, applying the Lithogeochemical Whole Rock Major and Trace Element analytical method. Total abundances of the major oxides and a few minor elements were reported on a .2 g sample analyzed by ICP emission spectrometry following a Lithium metaborate/tetraborate fusion and dilute nitric digestion. Total trace elements were analyzed by ICP mass spectrometry—refractory elements went through the same decomposition as the major elements (additional .2 g sample) while the rest were digested in hot Aqua Regia and analyzed by ICP MS (.5 g sample). Analytical work was subjected to the strictest quality control in the ACME Labs, with blanks, duplicates and standard reference materials (STD SO-18) included in the CQ report, together with a certificate of analysis, as a measure of

background noise, accuracy and precision. For the purpose of this work, the procedure for handling the data below the analytical detection limit (left-censored data) was accepted from Tarvainen et al. (2005) as the substitution method of assigning one-half of the detection limit value to censored data. This method is predominantly in use in geochemical and environmental studies (as per Antweiler and Taylor, 2008) developed from earlier works on analytical chemistry (e.g., Analytical Methods Committee, 1987).

Bulk mineralogy was determined by X-ray diffraction (XRD) analysis. XRD analysis was performed at the Croatian Geological Survey, on randomly oriented whole-rock powders using an X'Pert Powder X-ray diffractometer (Cu-Kα radiation, 45 kV, and 40 mA) at 2θ angles of 5˚–66˚ and a step size of .02˚. Mineral phases were identified from the XRD patterns using the ICDD PDF-4/Minerals database and the HighScorePlus software package.

Statistical analysis

Compositional data and log-ratio analysis

The bauxite data contain the set of 32-part geochemical compositions consisting of 10 major elements (represented as total
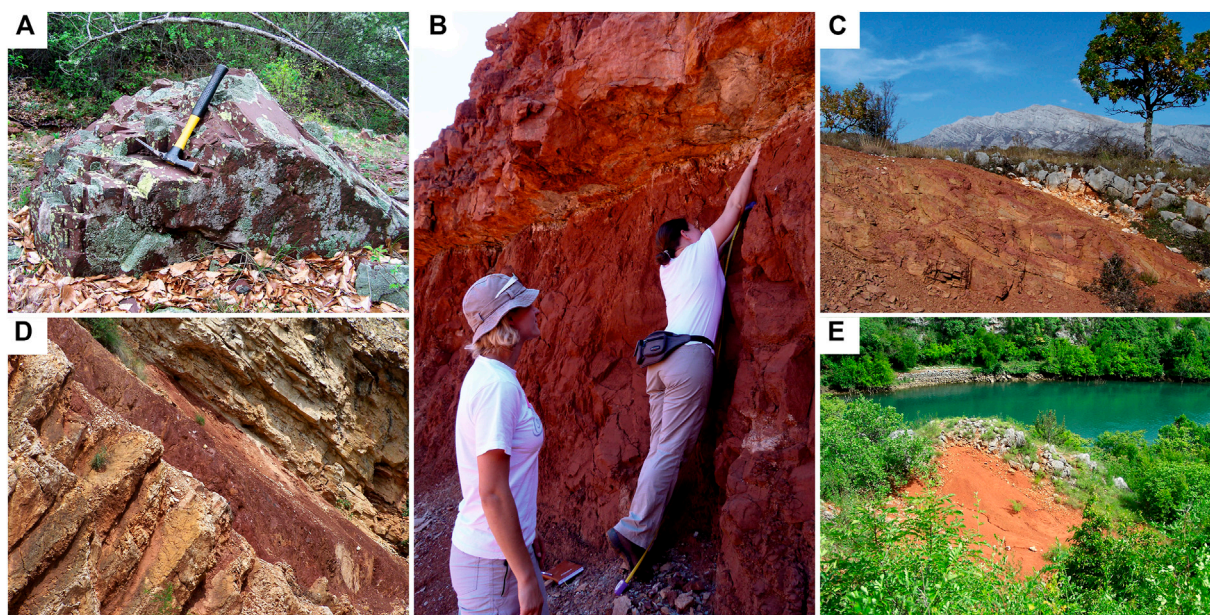
FIGURE 3
Field photographs of the typical bauxite-bearing horizons: **(A)** Upper Triassic bauxite (BX1) from Vrace deposit in the region of Lika. **(B)**. Sampling of the active Mondelako bauxite deposit near Rovinj (Istria), Upper Jurassic (Malmian) (BX2). **(C)** Outcrop of a typical small Lower Cretaceous bauxite deposit (BX3). Dinara Mt. is in the background. **(D)** Bauxite at the Upper Cretaceous (foraminiferal limestone)–Upper Eocene ("Promina beds") contact in the Northern Dalmatia (BX7). Underlying limestone beds show intense karstification. **(E)** Small outcrop of Miocene bauxite (BX8) at the bank of the Cetina River (Central Dalmatia).

abundances of major oxides) and 20 trace elements (Cr represented as Cr_2O_3) plus two rare-earth element groups summarized as light- and heavy rare earth elements (LREE = La+Ce+Pr+Nd+Sm; and HREE= Eu+Gd+Tb+Dy+Ho+Er+Tm+Yb+Lu) which were selected as predictor variables in building the original discriminant function model (DFM). The analyzed database includes 215 bauxite samples collected from bauxite deposits and occurrences over the entire Croatian part of ADCP, *a priori* separated in eight groups in accordance with their age (the age of hanging-wall rock formations). These comprise previously described horizons designated as the BX1—BX8 succession, from the lowest (Upper Triassic, BX1) to the highest (Miocene, BX8). Also, four samples of terra rossa soils (chromic luvisols) were included into the dataset as a control group (TR) keeping in mind that most karst bauxites have most probably originated by transformation of the soil-derived proto-bauxitic source material (terra rossa) as described earlier. These samples were selected as the most representative from the rich database collected during the multiyear regional geochemical survey based on the low-density topsoil sampling campaign over the karst region of Croatia (Halamić and Miko, 2009; Halamić et al., 2012; Hasan et al., 2020).

The whole rock composition of bauxite samples represents the classic example of compositional data (CoDa) in ore and environmental geochemistry. The nature of CoDa implies a mathematical property that all variables (compositions or component parts) in the analyzed sample are always positive values that must sum to a constant (unit value), usually expressed in percentages or mg/kg. As a result, all geochemical, mineralogical, and other datasets in the geoscience world are heavily plagued by the constant-sum constraint (CSC). This problem interferes with procedures of traditional statistics since individual variables are represented only as parts of some whole, or fractions of a constant sum, and cannot fluctuate independently (closed data) causing the presence of spurious correlations. Formally, CoDa cannot be represented in their raw form as points in the open, Euclidean space, where the scale is absolute, not relative. They refer to a restricted sample space known as simplex (simplicial complex) consisting of D parts or compositions (e.g., geochemical variables). Thus, a D-part composition (S^D) is really a subset of D-dimensional real space (R^D) and can be represented by the following expression (Pawlowsky-Glahn and Egozcue, 2007; Buccianti, 2013):

$$S^D = \left\{ (x_1, x_2, x_3, ..., x_D): x_i > 0 \, (i = 1, 2, 3, ..., D), \sum_{i=1}^{D} x_i = \kappa \right\}$$
$$(1)$$

where κ is a constraint-sum constant, $x_1, x_2, x_3, \ldots x_D$ are components of the composition x, and 1, 2, 3, ..., D are parts of the composition x.

Simplex can "inflate" into the Euclidean vector space structure only after the proper transformation is applied to its components. From an array of transformations introduced in the literature the centered log-ratio transformation (clr) of raw (compositional) data, originally proposed by Aitchison (1986) is used in this work. The application of the centered log-ratio is deemed essential for processing CoDa in the multivariate statistical methods such as discriminant function analysis since it preserves original distances between corresponding compositions allowing them to be handled straightforwardly (Egozcue and Pawlowsky-Glahn, 2006; Tolosana-Delgado, 2012). The singularity problem inherent to a clr-transformed covariance matrix could be circumvented if MDA operates on its reduced form, which is, not relying on a full rank of covariance (Daunis-i-Estadela et al., 2011). Since clr-transformed data represent unbounded real vectors in real space, in this case Mahalanobis distances (MD) stay invariant regardless of which component may be removed from the analysis (Barceló-Vidal and Pawlowsky-Glahn, 1999). Non-essential clr-transformed variables may be amalgamated ("other") and removed from further analysis.

Clr-coefficients can be computed from the following expression:

$$clr(x) = \left(\log \frac{x_1}{g(x)}, \log \frac{x_2}{g(x)}, \log \frac{x_3}{g(x)}, \ldots, \log \frac{x_D}{g(x)} \right) \quad (2)$$

where $x_1, x_2, x_3, \ldots x_D$ represent parts (compositions), and $g(x)$ represents the geometric mean of the parts.

However, as the compositional nature of geochemical data is expressed either in wt%, or in ppm, affecting the scale, all measurements are converted into ppm before transformation by multiplying wt% by 10^4.

Discriminant function analysis−building a predictive discriminant model (DFM)

Multiple (multi-group) discrimination analysis (MDA) is one of the traditional multivariate statistical techniques, which is particularly useful in building the predictive model of a multiple-group discrimination based on the set of independent (predictor) variables. In many of its practical considerations in geosciences MDA is frequently applied when geological reasoning asks for the use of some independent criterion for separation with respect to the variables in the analyzed dataset. It is a capable tool in manipulating a great number of numeric attributes alleviating problems with organization, distinction, or comparison of the vast body of data down to the scale providing a clearer insight into the underlying geological, geochemical or environmental controls. Also, the data processed in this way can develop a mapping property capable of further elucidating the intrinsic relationship among the original variables. As a statistical method it is effective in pursuing the major sources of between-group differences such as, in this case, tracking down the differences in the whole rock composition of Croatian ADCP bauxites emplaced in diverse paleogeographical/

paleotectonic settings during the Upper Triassic to Miocene times. Each bauxite horizon reflects a unique set of depositional platform dynamics making a regional marker of global events occurring at specific intervals in the stratigraphic record, a criterion autonomous with regards to the chemistry of hosted bauxite deposits. Objectives and principles of DA are described comprehensively in many statistical textbooks (e.g., Dillon and Goldstein, 1984; Davis, 1986; Rock, 1988; Reimann et al., 2008) and they were also regularly expounded by the same authors in various geochemical, environmental, sedimentological, bauxite and other studies (e.g., Peh et al., 2008; Kovačić et al., 2009; Peh and Halamić, 2010; Kovačević Galović et al., 2012; Peh and Kovačević Galović, 2014; Galović and Peh, 2016; Peh and Kovačević Galović, 2016; Grizelj et al., 2017; Šorša et al., 2018; Brunović et al., 2019; Hasan et al., 2020; Razum et al., 2020a; b, Razum et al., 2021). In this instance, MDA is envisaged to maximize the between-group variance in comparison to the variance within each group, classifying each individual sample into one of the *a priori* defined groups with minimum error rate (proportion of misclassified objects). Statistically, a hypothesis is tested that all observed groups have the same multivariate mean against the alternative that at least one multivariate mean is different (Rock, 1988). Provided that alternative hypothesis is accepted, the original suite of data is recalculated by MDA into a number of discriminant scores allocating each object or group (the latter represented by its mean) along one or more lines—linear discriminant functions. In this way the multivariate problem is reduced into a fewer-dimension solution, one less than the number of groups (K-1), or equal to the number of variables (p), whichever is smaller.

Consequently, the scope of this study revolves around building a predictive discriminant function model (DFM) with maximum classification efficiency which is based on eight *a priori* defined groups of ADCP bauxites (BX1—BX8) + one soil group (TR) and 32 log-ratio transformed CoDa geochemical variables (whole rock chemical analysis). For that purpose, a discriminant analysis from the statistical software package of STATISTICA, Release 7.1 (StatSoft, Inc., 2006) was used in order to achieve the best separation between the groups and explain the possible geological causes for the structure of input data by a single discriminant model. In the final analysis, this procedure implies the most effective transfer of mathematical (structure) model into a functional (geochemical) one, explaining post-hoc the analyzed dataset that is organized beforehand upon predictions.

Results

Weathering intensity in relation to mineralogical and geochemical characteristics

Mineralogical analysis based on XRD data revealed that the main oxy-hydroxides recorded in the most of the analyzed karst
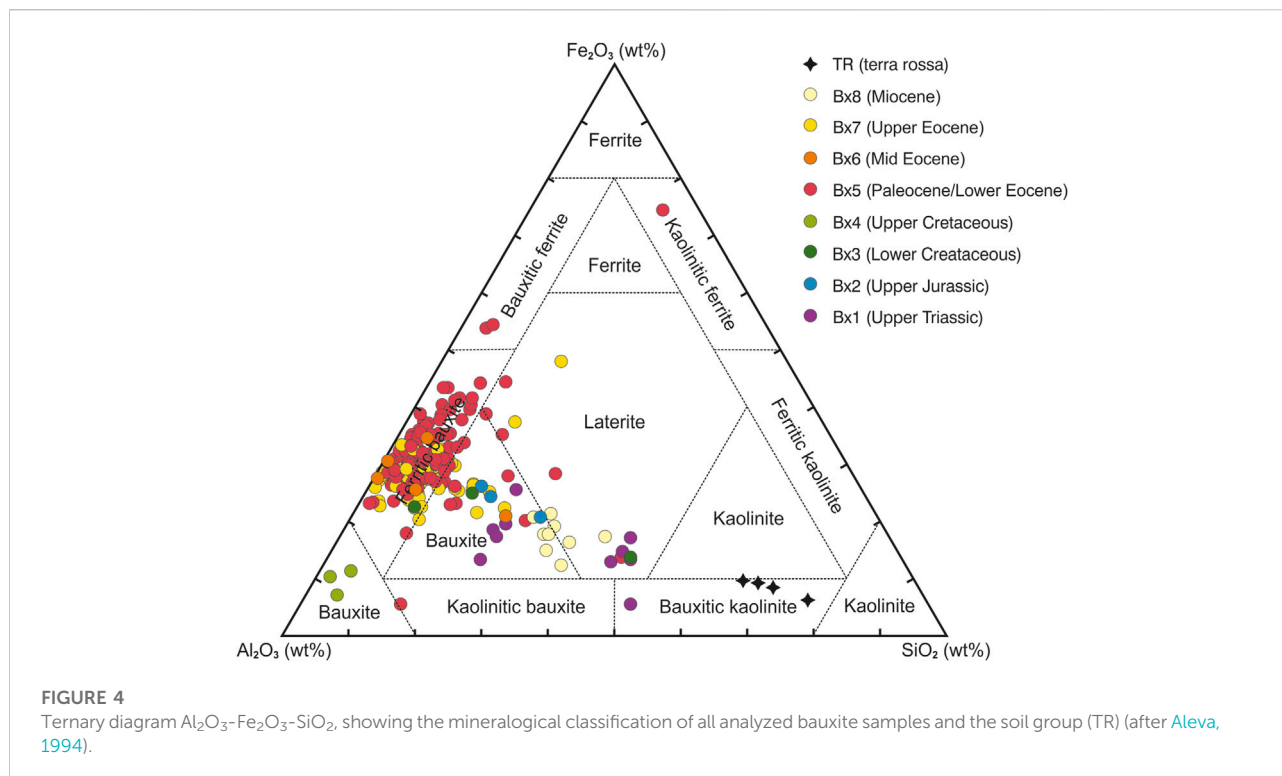
TABLE 1 Mineralogical composition of characteristic bauxite samples from each analyzed karst bauxite group.

Group	Age	Sample	Locality	Major minerals	Minor minerals
BX1	Upper Triassic	LI-5	Baške Oštarije (Lika)	Kaolinite	Böhmite, hematite, anatase
BX2	Upper Jurassic	ISTJ-1	Bralić (Istra)	Böhmite	Kaolinite, hematite, goethite, anatase
BX3	Lower Cretaceous	VRDK-1	Vrlika (N Dalmatia)	Böhmite	Kaolinite, hematite, goethite, anatase
BX4	Upper Cretaceous	KOR-3	Kordun (Banovina)	Böhmite	Goethite, anatase
BX5	Paleocene/Lower Eocene	IPC-53	Motovun (Istra)	Böhmite	Gibbsite, hematite, goethite, kaolinite, anatase
BX6	Middle Eocene	COS 2–1	Ćosići (Imotski)	Gibbsite	Hematite, goethite, böhmite, kaolinite, anatase
BX7	Upper Eocene	MB-4	Mamutovo brdo (Imotski)	Gibbsite, böhmite	Hematite, goethite, anatase, kaolinite
BX8	Miocene	SNG-7	Sinj (C Dalmatia)	Gibbsite, kaolinite	Anatase, 2:1 clay minerals

bauxite samples are böhmite and/or gibbsite, hematite, goethite and anatase (Table 1). Böhmite is the major mineral phase mainly in the samples from the oldest horizons (BX2-BX5), whereas gibbsite occur in younger bauxite horizons (BX5-BX8), sometimes associated with böhmite. In some bauxite samples calcite and/or quartz occur. The ubiquitous clay mineral is kaolinite, which occurs dominantly in the Upper Triassic (BX1) and Miocene (BX8) horizons. Additionally, some of the Upper Jurassic (BX2) and Miocene (BX8) bauxites contain other clay minerals belonging to the 2:1 clay minerals group, which were not analyzed in detail. In the samples from the youngest Miocene bauxite horizons (BX8), the böhmite mineral phase is absent or is present in small amounts. It was also determined in the study of Miocene bauxite deposit of Crveni Klanac in Dalmatia. Additionally, the Authors gave evidence of the 2:1 clay minerals presence in this bauxite ore of Miocene age (Brlek et al., 2021).

Whole-rock chemical analyses gather information on the concentrations of major (wt%), minor and trace elements (mg/kg) in bauxites and soils. As expected, Al_2O_3 and Fe_2O_3 contents are high in all bauxite samples (on average 47.06% and 22.32%, respectively), while SiO_2 and TiO_2 have average values of 7.51% and 2.56%, respectively. The higher CaO concentrations in several bauxite samples from Lower Paleogene (BX5), Upper Eocene (BX7) and Miocene (BX8) correspond to the samples in which the calcite is observed. The highest Al_2O_3 concentrations are evident in Upper Cretaceous bauxites (BX4) (67.57–70.58%), while for most of the horizons it ranges between ~30% and 60% (Upper Triassic–BX1, Upper Jurassic–BX2, Lower Cretaceous–BX3, Middle and Upper Eocene–BX6 and BX7). The bauxites from the Miocene–BX8 show the lowest values (22.57–39.73%), while the Lower Paleogene bauxites–BX5 have the highest oscillation between a minimum value of 4.52% and a maximum of 58.58%. Terra rossa/red soil samples, which are marked as group TR, show the lowest detected Al_2O_3 values between 14.07% and 19.02%. In contrast, their concentrations of SiO_2

are the highest, between 45.64% and 60.09%. Among bauxite horizons, the samples from Miocene bauxites–BX8 have the highest content of SiO_2 (from 20.46% to 29.92%). Considerably high values of SiO_2 are evident in bauxites from Upper Triassic–BX1 (18.42–41.33%), Upper Jurassic–BX2 (14.04–22.69%) and Lower Cretaceous–BX3 (7.03–36.92%), while the Lower Paleogene–BX5, Middle and Upper Eocene–BX6 and BX7 bauxites oscillate between the minimum and maximum values of .91–36.91% (BX5), .37–17.46% and .51–17.48% (BX7), respectively. The lowest contents of SiO_2 are detected in the Upper Cretaceous bauxites–BX4 (1.61–3.75%). The ternary diagram Al_2O_3-Fe_2O_3-SiO_2 (Figure 4, after Aleva, 1994) classified the analyzed bauxites as ferritic, especially the bauxite horizons of Lower Paleogene (BX5), Middle and Upper Eocene (BX6 and BX7). The Upper Cretaceous bauxites (BX4) are distinguished from the rest of the bauxite samples, as the ones with the highest Al_2O_3 and lowest Fe_2O_3 content. The terra rossa/red soils are characterized by the similar lower content of iron, with similar values of Fe_2O_3 as the Upper Cretaceous bauxites. The Upper Jurassic (BX2) and Lower Cretaceous (BX3), as well as part of the Upper Eocene (BX7), Miocene (BX8) and Upper Triassic (BX1) bauxites moved towards SiO_2 and kaolinite angle, implying moderate lateritization, but still belonging to bauxites and laterites, in contrast to kaolinite and bauxitic kaolinite classification of terra rossa/red soils (TR), which underwent weak lateritization. The chemical index of alteration (CIA; $[Al_2O_3/Al_2O_3+CaO+Na_2O+K_2O] \times 100$) values of all bauxite samples range between 90.83 and 99.90, with the lowest values in bauxite samples with increased CaO content that are detected in several bauxite samples from Upper Jurassic (BX2) and Upper Eocene (BX7) horizons. In general, CIA values show low variability for all bauxite horizons (>90) and indicate a significant chemical weathering during bauxitization (Nesbitt and Young, 1982). Terra rossa/red soil samples (TR) have values between 75.16 and 86.89, which reflects a lower degree of weathering where only kaolinitization occurred without the formation of bauxite mineral gibbsite.

FIGURE 4
Ternary diagram Al₂O₃-Fe₂O₃-SiO₂, showing the mineralogical classification of all analyzed bauxite samples and the soil group (TR) (after Aleva, 1994).

Discrimination of bauxite horizons

Descriptive statistics for the whole data set prior to data transformation and subsequent multivariate statistical procedure is summarized in Figure 5 containing the categorized box-and-whisker plots (boxplots by group) that represent univariate statistics of geochemical data (descriptor variables—Min-Max; Median; 1st and 3rd Quartile) for each bauxite horizon. Additionally, results of the MDA are briefly recapitulated in Table 2 containing: a) the multivariate test for the overall significance of discrimination and; b) the tests of residual roots (discriminant functions). The Wilks'λ statistical test, employed routinely in the analysis, shows the vanishingly low probability ($p<.000$) confirming that all bauxite groups have the same multivariate mean—a precondition required to safely proceed with computing discriminant functions (DFs). Since the number of groups in the studied case amounts to nine (including the group of four topsoil samples) (K=9) the between-group variation is completely explained by the eight discriminant functions (K–1). However, despite the high statistical significance of the variation between the observed groups (p-level in Table 2), only a smaller number of DFs is used in further analysis to explain the natural between-group variation. In fact, statistical significance is often of little use if the geological explanation, supported by the high 'a posteriori' classification rates, given in the initial assignments, is not readily available (Rock, 1988). Accordingly, labeling

discriminant functions in terms of processes is an essential part of the analysis because it provides the geologically meaningful interpretation of the entire discrimination scheme. This procedure allows the underlying mathematical structure of the analyzed geochemical observations to be disclosed to the investigator. Discriminant loadings (simple correlations of variables with respective DFs) are particularly useful in clarifying individual contribution of each descriptor variable (chemical element) to the overall discrimination, highlighting the geologic processes thought to be fundamentally responsible for the pattern of the functional, that is, a mathematically expressed geologic model. When constructing the optimal discriminating design, a number of variables with small discriminant loadings can be discarded from the model. To this purpose the variable diagrams (Figure 6A) provide the quickest and most informative insight into the structure of the discriminant space suggesting which variables (descriptors) would be retained to explain the meaning of the discriminant functions, as well as which subset of variables most clearly separates the previously defined groups. Further, the association among descriptor variables and related groups can be best displayed geometrically, considering DFs as axes in the reduced discriminant space. However, in this work the clr-transformed variable and groups are displayed on scatterplots instead of bi-plots as their multivariate analogs because the origin of the bi-plot can no longer correspond to the geometric mean of the dataset after omitting the amalgamated variable ("other") in
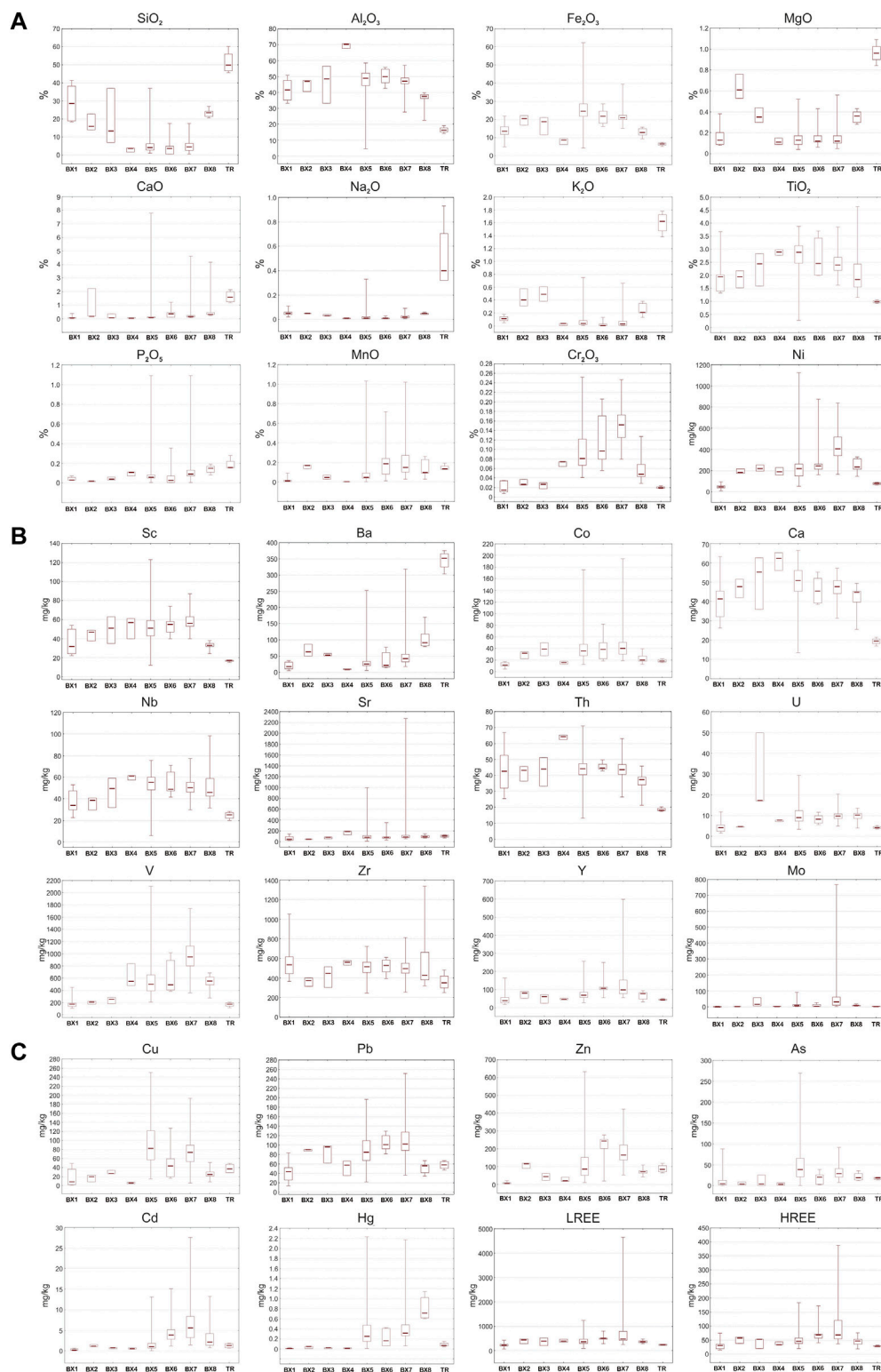
FIGURE 5
Box-and-whisker plots by groups, which represent univariate statistics of geochemical data (descriptor variables—min-max; median; and first and third quartile values) for each karst bauxite horizon (BX1-BX8) and soils (TR): **(A)** The abundances of major elements (expressed in %) and Ni (expressed in mg/kg). **(B)** The abundances of trace elements (expressed in mg/kg): Sc, Ba, Co, Ga, Nb, Sr, Th, U, V, Zr, V, Mo. **(C)** The abundances of trace elements (expressed in mg/kg): Cu, Pb, Zn, As, Cd, Hg, and LREE and HREE.

TABLE 2 Multivariate test for overall significance of discrimination (a) and tests of residual roots (b).

a)	
No. Of variables	32
Wilks' lambda	.0005
Approximate F ratio	9.052
Degrees of freedom	[256; 1,409]
p-level	$p < .000$

b)							
DF	Eigen value	Eigen (%)	Eigen cum	Canon. R	Wilks' λ	Chi^2	df	p-level
1	8.504	45.37	45.37	.946	.001	1493.9	256	.000
2	4.763	25.41	70.78	.909	.005	1049.2	217	.000
3	1.909	10.18	80.96	.810	.028	703.3	180	.000
4	1.625	8.67	89.63	.787	.083	492.4	145	.000
5	.759	4.05	93.68	.657	.217	301.8	112	.000
6	.633	3.38	97.06	.622	.382	190.2	81	.000
7	.425	2.27	99.33	.546	.623	93.4	52	.000
8	.126	.67	100.00	.335	.888	23.5	25	.547

order to compensate for matrix ill-conditioning. The scatterplot of variable loadings (Figure 6A) represents discriminant axes as normalized vectors, while the scatterplot of individual objects (Figure 6B) defines the same as discriminant score vectors. Affiliation between variables and groups is examined using their corresponding position along the relevant axis which is vital for overall separation of groups and subsequent transfiguration of functional (structural) into a process model. Each DF contributes to a single geologic process responsible for the separation while the variables participate in this structure-process conversion as the building blocks assuming the role of process descriptors. In bipolar instances, though, where variables are united in negative relationship caution is required in the model assessment since the interpretation of variable-group interplay may not always be straightforward.

Discussion

Bauxites as provenance, climate and tectonics indicators

Labelling discriminant space (defined by K-1 DFs) is of paramount importance in MDA since it opens the way to recognition of the unseen relationships between the grouped data. Thus, the natural processes can be deduced, underlying the

mathematical structure of geochemical observations. In this case, the first three discriminant functions (DF1-DF3) deserve the closer inspection since, collectively, they account for more than 80% of the total between-group difference in the computed model (Table 2). As seen from the scatterplot of variable loadings (Figure 6A), all considered DFs are bipolar owing to their key variables mutually polarized on respective diagrams, although the importance of some groups is not equally emphasized (Figure 6B). In the case of DF1 explaining almost half of the total variability (over 45%), it can be readily interpreted as an image of the inverse relationship between the suite of elements representing the building blocks of clay minerals—major elements SiO_2, Al_2O_3, MgO, K_2O, Na_2O, followed by Fe_2O_3, TiO_2, Zr, Th, Sc and others—against another suite of elements represented by trace elements, heavy metals in particular, including Cr_2O_3, Ni, Zn, Mo, Hg and others. Inspection into the scatterplots (Figures 6A, B) reveals a characteristic transition from former to the latter suite directly related to the ADCP environmental changes from the Late Triassic to the Miocene times. This pattern is in sharp contradistinction to earlier investigations focused only on Lower Paleogene bauxites (Kovačević Galović et al., 2012; Peh and Kovačević Galović, 2014; Peh and Kovačević Galović, 2016), where major elements did not contribute appreciably in the model configuration. It was suggested that within a particular bauxite-formation period observed *per se*, such as the Early
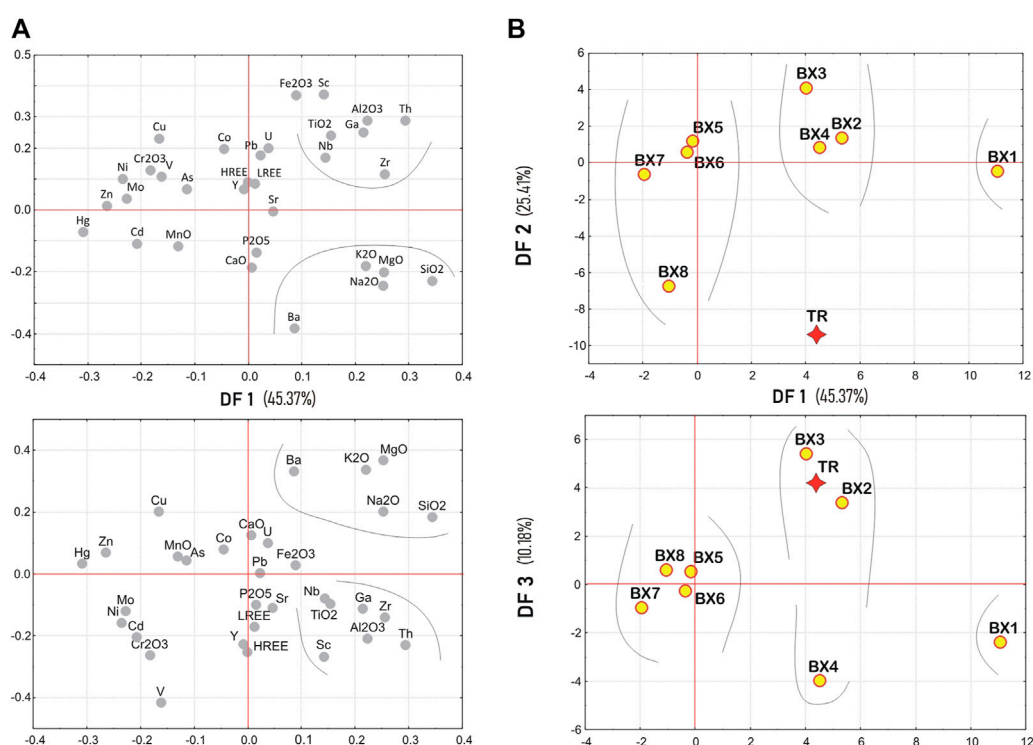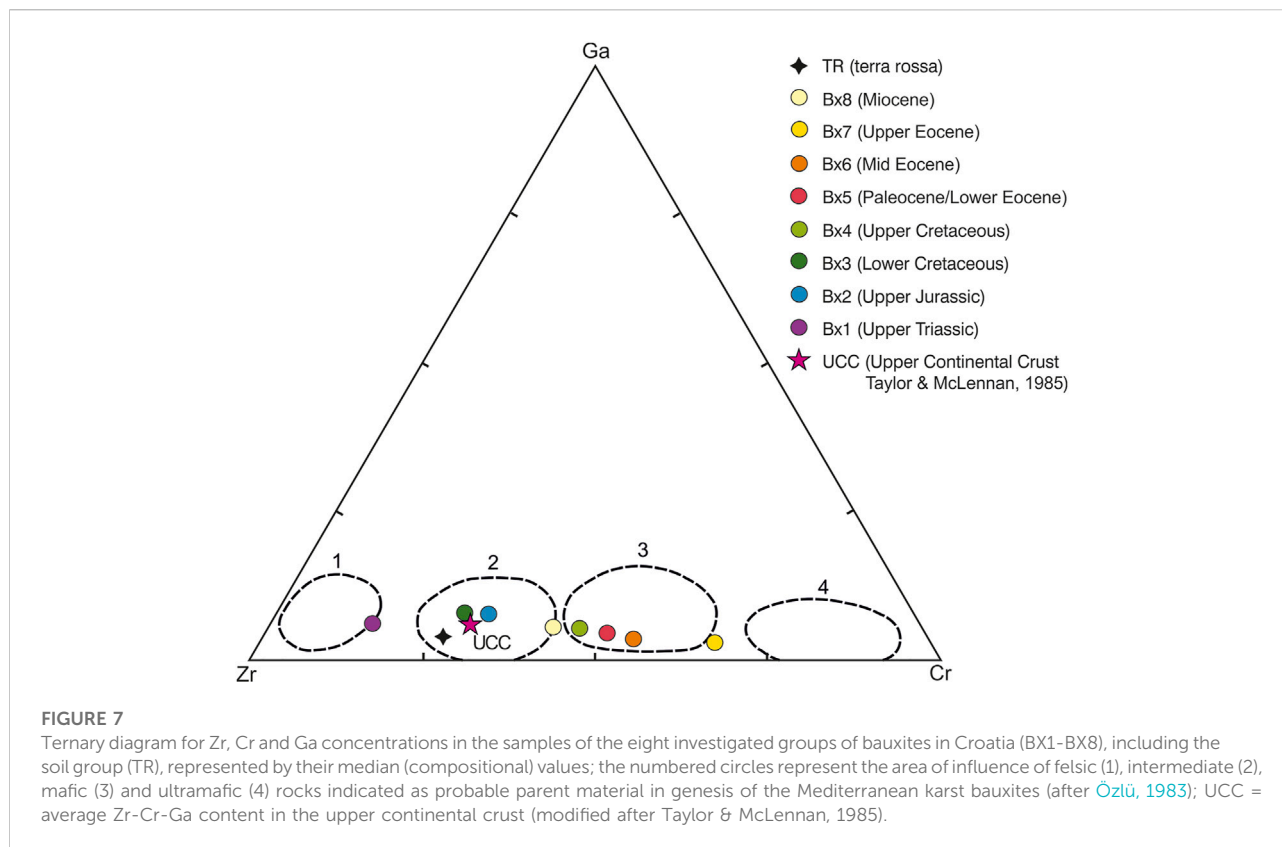
FIGURE 6
Comparison between variables and groups in the discriminant function model (DFM) of the clr-transformed data: scatterplots of **(A)** variable loadings and **(B)** bauxite groups in the reduced discriminant space of the first three discriminant functions (DF1−DF2 and DF1-DF3).

Paleogene, major elements performed a key role in all processes operating during sedimentary cycle (from weathering to burial to diagenesis) while minor and trace elements typically indicated a particular section of a cycle. Here, a temporal axis is involved into the tectonostratigraphic scheme indicating changing paleogeography and depositional dynamics on the evolving ADCP through the Upper Triassic—Miocene times. It is obvious from the variable-group scatterplots (Figures 6A, B) that bauxite groups make distinct clusters of which the Upper Triassic bauxites (BX1) forms a standalone unit characterized by an excessive amount of basic clay-mineral components, SiO$_2$ in particular. The cluster in the middle, encompassing Jurassic to Upper Cretaceous groups (BX2—BX4), shows the transition from "extreme" to "normal" bauxite geochemical composition represented by elements clustering around the central axis (CaO, P$_2$O$_5$, Y, LREE, HREE), as well as those slightly deviating in both directions (Sr, Pb, U, Co and others) thus signifying the "average" geochemistry of ADCP bauxites. The latter is characteristic of the youngest bauxite groups (BX5—BX8) formed from the Early Paleogene to the Miocene. In process terms, it may be assumed that DF1, along the BX1→BX8 time arrow, confronts the products of strong weathering precipitated in vadose (well-oxygenated) environments (BX1) with the bulk of trace elements present only in small quantities with respect to

younger bauxite horizons (set on the opposite pole of the variable diagram) (Figure 5; Figure 6A). To this may be added that Nb, Zr, and Ga in particular, straightforwardly indicate hydrous conditions where bases were effectively leached in primary (proto) bauxite material (from right to left pole of DF1, Figure 6A). Otherwise said, durability of hiatuses, input of different material (detrital or residual) and changing environmental conditions (e.g., discontinued leaching as a result of changing climate or drainage conditions) (Kovačević Galović et al., 2012) together with later burial and diagenetic processes may have affected different bauxite horizons geochemically exactly as observed in the computed model—through the process of leaching being increasingly less effective in time (BX1→BX8). Another implication arising, following from DF1 structure is the inference of the precursor rock types as the bauxite parent material. A sharply polarized relationship between the two abovementioned sets of elements loaded on DF1 speaks strongly in favor of changing provenance of the source material, shifting steadily from felsic to mafic/ultramafic from the Upper Triassic to Miocene times. Also, potential precursor rock types can be easily deduced from the ternary diagram contrasting the Cr, Zr and Ga concentration values (compositions) of all bauxite groups (Figure 7) (Özlü, 1983). Chromium is typically enriched in ultramafic and mafic rocks and its elevated values in bauxites

FIGURE 7
Ternary diagram for Zr, Cr and Ga concentrations in the samples of the eight investigated groups of bauxites in Croatia (BX1–BX8), including the soil group (TR), represented by their median (compositional) values; the numbered circles represent the area of influence of felsic (1), intermediate (2), mafic (3) and ultramafic (4) rocks indicated as probable parent material in genesis of the Mediterranean karst bauxites (after Özlü, 1983); UCC = average Zr-Cr-Ga content in the upper continental crust (modified after Taylor & McLennan, 1985).

suggest ophiolitic complexes containing ultramafics and related rocks as a parent material (DeVos et al., 2006). Together with other trace elements, such as Ga and Zr in particular (indicative, though, for felsic and intermediate rocks), which are considered immobile during weathering and hydrothermal alteration processes (MacLean and Barret, 1993), the ratios that Cr forms in bauxites do not differ greatly from those in parent rocks (Valeton et al., 1987) and therefore can be applied in bivariate or ternary diagrams for the determination of the parent rocks. Thus, the ternary diagram of Zr-Cr-Ga concentrations of Croatian ADCP karst bauxites (Figure 7) indicate that Upper Triassic (BX1) bauxite parent material could be traced to felsic or intermediate rocks, while Upper Jurassic (BX2) and Lower Cretaceous (BX3) bauxites that closely conform to average upper continental crust (UCC) are probably derived from intermediate rocks. Parent material for the Upper Cretaceous (BX4), Lower Paleogene (BX5), and Middle Eocene (BX6) were possibly mafic rocks, while Upper Eocene (BX7) bauxites show a shifting towards ultramafic values for chromium. Exception is, however, the youngest, Miocene bauxite (BX8), being placed on the verge of the intermediate rock cluster (Figure 7), indicating a provenance signature more typical for intermediate rocks. Note also that the oldest, Upper Triassic bauxites indicate an affinity of the precursor material with felsic (estimated from both weighted averages of surface samples and studies of

shales and loess, as per Rudnick and Gao, 2013), rather than mafic rocks in the incipient stages of the ADCP development. Thus, the ternary diagram stands in support of the provenance issues indicated by the presence of still other "conservative" elements such as Nb and Th in the original MDA model attending SiO_2–Al_2O_3–Fe_2O_3 elemental cluster (Figure 6A).

Soils (terra rossa), included in the analysis as a control group (TR) due to the widely accepted idea that they represent detritally- or residually-derived proto-bauxitic material subsequently transformed, are clearly separated from other bauxite groups. Their proper nature, however, is decidedly explained only after the examination of DF2.

Most of the residual variation left after eliminating DF1 from further analysis is carried by the second discriminant function DF2 (over 25%) whose distinct property is separation of BX8 and TR groups from the rest, especially BX3, implying that Miocene bauxites are most different geochemically from all other bauxite groups, notably the Lower Cretaceous ones. The particularity of DF2 is that it highlights the TR group (the red soils) as the supposed proto-bauxite material formed in the incipient stage of subaerial exposure and interaction between karstified carbonate bedrock and airborne material (aeolian dust or volcanic ash) (Merino and Banerjee, 2008; Šušteršič et al., 2009; Banerjee and Merino, 2011), in a sheer contradistinction

TABLE 3 Classification matrix.

Groups	BX1	BX2	BX3	BX4	BX5	BX6	BX7	BX8	TR	% correct
BX1	10	0	0	0	0	0	0	0	0	100.00
BX2	0	3	0	0	0	0	0	0	0	100.00
BX3	0	0	3	0	0	0	0	0	0	100.00
BX4	0	0	0	3	0	0	0	0	0	100.00
BX5	0	0	0	0	101	1	7	0	0	92.66
BX6	0	0	0	0	1	3	1	0	0	60.00
BX7	0	0	0	0	1	1	71	0	0	97.26
BX8	0	0	0	0	0	0	0	9	0	100.00
TR	0	0	0	0	0	0	0	0	4	100.00
Total	10	3	3	3	103	5	79	9	4	94.52

Rows: Observed classifications (samples lost to other groups).
Columns: Predicted classifications (samples obtained from other groups).

TABLE 4 Squared Mahalanobis distances (SMD) between the bauxite groups (BX1—BX8) and soil (TR).

	BX1	BX2	BX3	BX4	BX5	BX6	BX7	BX8	TR
BX1	.00	107.30	193.58	125.27	139.04	148.56	174.84	205.49	187.01
BX2	107.30	.00	76.90	124.17	74.61	69.01	101.24	156.29	166.10
BX3	193.58	76.90	.00	149.63	112.31	121.91	142.58	221.12	262.47
BX4	125.27	124.17	149.63	.00	102.43	97.82	106.91	169.44	234.10
BX5	139.04	74.62	112.31	102.43	.00	11.52	11.65	72.11	160.14
BX6	148.56	69.01	121.91	97.82	11.52	.00	13.18	71.86	167.67
BX7	174.84	101.24	142.58	106.91	11.65	13.18	.00	53.21	156.85
BX8	205.49	156.29	221.12	169.44	72.11	71.66	53.27	.00	94.27
TR	187.01	166.10	262.47	234.10	160.14	167.67	156.85	94.27	.00

to all bauxite groups except BX8 (Miocene). This contrast is based on the strong presence of alkali and alkaline earth elements as building blocks of clay minerals—SiO_2, K_2O, Na_2O and MgO in modern terra rossa soils still intact by the process of bauxitization. Here, Ba is highlighted owing to its sorption behavior on clay minerals, probably a characteristic of regional soils in the Dinaric region, mostly soils derived from siliciclastic material and developed in mountainous/sub-mountainous areas (Halamić and Miko, 2009; Halamić et al., 2012; Hasan et al., 2020). In this sense the Miocene bauxites (BX8), as the latest products of bauxitization in the Croatian karst Dinarides, depart only slightly geochemically from modern soils. On the other side of the scale are all the other groups characterized by a higher content of alumina and associated elements (Fe_2O_3, TiO_2, Sc, Th, Ga . . .), while being more or less depleted in clay

components prevalent in BX8 and TR groups. In process terms, DF2 can be easily described as the function of ferralitization, or, more typically desilication which includes removal of silica from primary silicates and even from quartz, and leaving the protobauxite material enriched with accumulated (hydr) oxides of Fe and Al (van Breemen and Buurman, 1988), involving also the noticeable depletion of basic cations. Mark, however, that positive values of discriminant coefficients (canonical means) keep all bauxite groups except BX8 close to the zero line implicating the "unfinished" process of chemical weathering during short, punctuated episodes of subaerial exposure.

Above said, it is exactly DF3, explaining the residual 10% of total variance (Table 2), that underscores a more complete loss of alkali and alkaline earth cations and SiO_2 by desilication, during intense weathering and subsequent

transformation of protobauxite material. As an inverse image of DF2, it highlights the Upper Cretaceous bauxites (BX4) as aluminum-rich bauxite with over 70% of Al_2O_3 (Figure 5), together with increased quantities of Th, Sc, Cr_2O_3, V, as well as Y and HREE, LREE. Similarly to DF2, DF3 can be interpreted as an indicator of extensive leaching of silica under extreme weathering conditions in hot and wet climate, analogous to those observed in the modern tropics and sub-tropics. However, it also involves the process of deferralitization since, unlike DF2, Fe2O3 is not the part of the Al_2O_3–Fe_2O_3–TiO_2–Th– . . . cluster, setting close to the zero line without any discriminatory potential (Figure 6). This process occurs in acidolytic environments, due to organic accumulation in weathering profiles in well-drained areas in a cool and humid climates, where all cations tend to be removed from the minerals (Chamley, 1989). Reducing conditions cause the dissolution of Fe oxides and Fe depletion in such environments (Do Nascimento et al., 2008). As the process of deferralitization in modern soils usually occurs through the production of soluble organic or inorganic complexes in extremely humid and well drained regions of the world, it may be assumed as the potential mechanism of iron leaching from protobauxites during weathering (e.g., Thiffault, 2019). Though kaolinite and bauxite deposits are considered to have been formed under humid tropical and subtropical conditions, kaolinite can form in cool temperate climates under moderate rainfall. For appreciable thickness to form, long periods of leaching are required. Less time is required in warmer regions, which is probably why the larger kaolin and bauxite deposits are restricted to the warmer climates. Additionally, it is necessary to have a relatively smooth terrain and quiet tectonic conditions so that chemical weathering can be more effective than erosion (Weaver, 1989), which corresponds to long-lasting emersion during the Upper Cretaceous, with a low-developed karst paleorelief where small Upper Cretaceous bauxite deposits occur in the Croatian part AdCP. DF3 discriminates the Upper Cretaceous (Senonian) as the only time period (epoch) having experienced the optimum bauxitiferous conditions in the Croatian part of ADCP, albeit resulting with small and rare deposits (Šinkovec et al., 1985).

Classification issues

Concerning the integrity of investigated groups, it is once again the classification efficiency that demonstrated its usefulness in the process of discrimination. In this regard, classification rates of *a priori* defined bauxite groups can be readily inspected by comparing the mathematically "predicted" (computed) and original ("natural") group membership of individual samples. Table 3 reveals that the discriminant model is organized with an extremely high efficiency of almost 95%. Setting aside Upper Triassic bauxites (BX1) that are literally "miles away" geochemically from any of the remaining bauxite groups, a fact

obvious from the very high values of squared Mahalanobis distance (SMD) ranging from 107.30 for Jurassic (BX2) up to 205.49 for Miocene bauxites (Table 4), there is a great affinity between the three Paleogene groups—BX5, BX6 and BX7. Their SMD values range between 11.65 and 13.18 revealing similar climatic and tectonostratigraphic constrains during the punctuated episodes of Paleogene subaerial exposure over the entire Croatian part of ADCP. Three groups form a characteristic cluster mentioned before, and there is only a slight mingling of their members that may call for closer inspection into the age of hanging-wall formations, especially in the case of the Middle Eocene group (BX6). All other groups are correctly classified (100%) with notable distances among the groups forming the Jurassic-Cretaceous cluster ranging in SMD from minimally 76.90 (BX2/BX3) to maximum of 149.63 (BX3/BX4). As expected, the soils (TR) are the most distant of all bauxite groups representing an entity *per se*. Unsurprisingly, however, some affinity with Miocene bauxites (BX8), as indicated by DF3 (Figures 6A, B), is strongly validated by SMD values standing halfway to all other groups (BX1-BX7) (Table 4), mostly due to the high contents of silica and base cations ineffectively leached during bauxitization (Table 1).

Conclusion

In this study, a discriminant function model was built with the aim of distinguishing geochemically between the eight bauxite horizons ranging from the Upper Triassic to the Miocene and sampled from the various corners of the Croatian part of ADCP. Having derived their origin from various regional unconformities bauxites were supposed to have experienced different formation settings as regards both regional (volcanism and tectonics), and global (eustasy and climate), controls during the periods of subaerial exposure of the platform. From this perspective, their emplacement on carbonate platforms such as ADCP represents a rich data repository of valuable information on predicting depositional and diagenetic facies during geological history. Leaving aside possible rearrangements of control factors that may have generated variations as regards some specific bauxite horizon (horizontal, or within-period, causality) most notably articulated in flexural uplift and progressive formation of the forebulge unconformity in Istria during Lower Paleogene times, the focus of this research was given to changes in time (vertical causality) presumed to be of major importance in setting down the bauxite geochemical signature. Accordingly, although investigations presented in this work are targeted locally in spatial sense (Croatian part ADCP) results of MDA are pursued over the considerable timespan, that is, if oxymoron is apt in this case, non-locally in time, which may touch upon a sort of uniqueness in the bauxite studies. The results can be briefly summarized as follows:

1) Almost complete separation between the eight groups (horizons) of Croatian karst bauxites from various parts of ADCP (Inner

and Outer Karst) is accomplished by applying MDA on the set of 32-part geochemical compositions. Typically, only the Paleogene cluster (BX5–BX6–BX7) exhibits certain inconsistencies identified in mutual replacement of their members, notably between the Lower Paleogene and Upper Eocene groups. These, however, may well be elicited by the geochemical affinity between the groups in cases where the hanging wall sediments have been removed and relative age-dating by geological mapping was only inferential. Emplacement of older (BX1–BX4) and younger (BX8) bauxite horizons on ADCP left their geochemical imprint entirely individualized during the platform depositional history, most probably due to characteristic tectonostratigraphic controls predominant at each particular regional unconformity.

2) Three discriminant functions comprising over 80% of total variability are interpreted in terms of typical bauxite-forming processes on the ADCP subaerial exposure surfaces. DF1 is by far predominant (over 45%) signaling change in the bauxite geochemical record since the Upper Triassic (BX1) to Miocene (BX8) times caused by the complex interplay of changeable vadose–phreatic bauxite-forming karst paleo-environments and a progressively more emphasized input of mafic precursor material into the composition of deposited proto-bauxites. The other two discriminant functions (DF2-DF3) comprising further 25% and 10%, respectively, of the total model variance portray the processes of progressive ferralitization (DF2) and, finally, desilication (DF3) leaving ultimately Upper Cretaceous bauxites (BX4) as the most thoroughly "developed" bauxites with very high content of alumina (Med=70.29%) and very low content of silica (Med=3.66%), the latter on a par only with Paleogene bauxites (BX5-BX7). The geochemical signal of the modern soils (TR) corroborates the idea of their role in the genesis of karst bauxites as witnessed by the close ("half-way") relationship with the youngest bauxite group BX8 on DF2.

Data availability statement

The raw data supporting the conclusions of this article will be made available by the authors, without undue reservation.

References

Abedini, A., Khosravi, M., and Calagari, A. A. (2018). Geochemical characteristics of the Arbanos karst-type bauxite deposit, NW Iran: Implications for parental affinity and factors controlling the distribution of elements. *J. Geochem Explor* 200, 249–265. doi:10.1016/j.gexplo.2018.09.004

Abedini, A., and Khosravi, M. (2020). Geochemical constraints on the Triassic–Jurassic Amir-Abad karst-type bauxite deposit, NW Iran. *J. Geochem Explor* 211, 106489. doi:10.1016/j.gexplo.2020.106489

Aitchison, J., and Egozcue, J. J. (2005). Compositional data analysis: Where are we and where should we be heading? *Math. Geol.* 37, 829–850. doi:10.1007/s11004-005-7383-7

Author contributions

Funding

Acknowledgments

Conflict of interest

The authors declare that the research was conducted in the absence of any commercial or financial relationships that could be construed as a potential conflict of interest.

Publisher's note

All claims expressed in this article are solely those of the authors and do not necessarily represent those of their affiliated organizations, or those of the publisher, the editors and the reviewers. Any product that may be evaluated in this article, or claim that may be made by its manufacturer, is not guaranteed or endorsed by the publisher.

Aitchison, J. (1982). The statistical analysis of compositional data. *J. Roy. Stat. Soc. Ser. B* 44, 139–160. doi:10.1111/j.2517-6161.1982.tb01195.x

Aitchison, J. (1986). *The statistical analysis of compositional data*. London-New York: Chapman & Hall. doi:10.1002/bimj.4710300705

Aleva, G. J. J. (1994). *Laterites: Concepts, Geology, morphology and chemistry*. The Netherlands, Wageningen: International Soil Reference and Information Center.

Analytical methods committee (1987). Recommendations for the definition, estimation and use of the detection limit. *Analyst* 112, 199–204. doi:10.1039/an9871200199

Antweiler, R. C., and Taylor, H. E. (2008). Evaluation of statistical treatments of left-censored environmental data using coincident uncensored data sets: I. Summary statistics. *Environ. Sci. Technol.* 42, 3732–3738. doi:10.1021/es071301c

Banerjee, A., and Merino, E. (2011). Terra rossa Genesis by replacement of limestone by kaolinite. III. Dynamic quantitative model. *J. Geol.* 119, 259–274. doi:10.1086/659146

Barceló-Vidal, C., and Pawlowsky-Glahn, V. (1999). Letter to the editor: Comment on "singularity and nonnormality in the classification of compositional data" by Bohling GC, Davis JC, Olea RA, Harff J. *Math. Geol.* 31, 581–585.

Bardossy, G. (1982). *Karst bauxites: Bauxite deposits on carbonate rocks.* Budapest: Akadémiai Kiadó.

Blašković, I., Dragičević, I., and Pokrajčić, I. (1989). *Tectonic control of the origin of the paleorelief of bauxite deposits in the Western Herzegovina, Yugoslavia*, 19/22. Travaux ICSOBA, 231–238.

Boni, M., Reddy, S., Mondillo, N., Balassone, G., and Taylor, R. (2012). A distant magmatic source for Cretaceous karst bauxites of Southern Apennines (Italy), revealed through SHRIMP zircon age dating. *Terra nova.* 24, 326–332. doi:10.1111/j.1365-3121.2012.01068.x

Boni, M., Rollinson, G., Mondillo, N., Balassone, G., and Santoro, L. (2013). Quantitative mineralogical characterization of karst bauxite deposits in the southern Apennines, Italy. *Econ. Geol.* 108, 813–833. doi:10.2113/econgeo.108.4.813

Brlek, M., Gaynor, S. P., Mongelli, G., Bauluz, B., Sinisi, R., Brčić, V., et al. (2021). Karst bauxite formation during Miocene climatic optimum (central Dalmatia, Croatia): Mineralogical, compositional and geochronological perspectives. *Int. J. Earth. Sci.* 110, 2899–2922. doi:10.1007/s00531-021-02091-z

Brlek, M., Korbar, T., Košir, A., Glumac, B., Grizelj, A., and Otoničar, B. (2014). Discontinuity surfaces in Upper Cretaceous to Paleogene carbonates of central Dalmatia (Croatia): Glossifungites ichnofacies, biogenic calcretes, and stratigraphic implications. *Facies* 60, 467–487. doi:10.1007/s10347-013-0378-9

Brunović, D., Miko, S., Ilijanić, N., Peh, Z., Hasan, O., Kolar, T., et al. (2019). Holocene foraminiferal and geochemical records in the coastal karst dolines of Cres Island, Croatia. *Geol. Croat.* 72 (1), 19–42. doi:10.4154/gc.2019.02

Buccianti, A. (2013). Is compositional data analysis a way to see beyond the illusion? *Comp. Geosci.* 50, 165–173. doi:10.1016/j.cageo.2012.06.012

Buccianti, A., Mateu-Figueras, G., and Pawlowsky-Glahn, V. (Editors) (2006). *Compositional data analysis in the geosciences: From theory to practice* (London: Geol. Soc. Spec. Publ.), 264.

Chamley, H. (1989). *Clay sedimentology.* Berlin: Springer.

Crampton, S. L., and Allen, P. A. (1995). Recognition of forebulge unconformities associated with early stage foreland basin development; example from the North Alpine foreland basin. *AAPG Bull.* 79, 1495–1514.

D'Argenio, B., and Mindszenty, A. (1995). Bauxites and related palaeokarst: Tectonic and climatic event markers at regional unconformities. *Eclogae Geol. Helv.* 88, 453.

D'Argenio, B., and Mindszenty, A. (1992). Tectonic and climatic controls on paleokarst and bauxites. *Giorn. Geol.* 54 (1), 207.

Daunis-i-Estadella, J., Thió-Henestrosa, S., and Mateu-Figueras, G. (2011). "Two more things about compositional biplots: Quality of projection and inclusion of supplementary elements," in *Proceedings of the 4th international workshop on compositional data analysis (CoDaWork 2011)*. Editors J. J. Egozcue, R. Tolosana-Delgado, and M. I. Ortego (Girona, Spain: Universitat de Girona), 1–14.

Davis, J. C. (1986). *Statistics and data analysis in Geology.* 2nd ed. New York: John Wiley & Sons.

De Vos, W., Tarvainen, T., Salminen, R., Reeder, S., De Vivo, B., Demetriades, A., et al. (Editors) (2006). "Geochemical atlas of Europe," *Part 2 – interpretation of geochemical Maps, additional tables, figures, Maps, and related publications* (Espoo: Geological Survey of Finland).

Dillon, W. R., and Goldstein, M. (1984). *Multivariate analysis: Methods and applications.* New York: John Wiley & Sons.

Do Nascimento, N. R., Fritsch, E., Bueno, G. T., Bardy, M., Grimaldi, C., and Melfi, A. J. (2008). Podzolization as a deferralitization process: Dynamics and chemistry of ground and surface waters in an acrisol – podzol sequence of the upper Amazon Basin. *Eur. J. Soil Sci.* 59 (5), 911–924. doi:10.1111/j.1365-2389.2008.01049.x

Durn, G., Aljinović, D., Crnjaković, M., and Lugović, B. (2007). "Heavy and light mineral fractions indicate polygenesis of extensive terra rossa soils in Istria, Croatia," in *Developments in sedimentology, Heavy minerals in use.* Editors M. A. Mange and D. T. Wright (Amsterdam: Elsevier), 701–737. doi:10.1016/S0070-4571(07)58026-3

Durn, G., Ottner, F., and Slovenec, D. (1999). Mineralogical and geochemical indicators of the polygenetic nature of terra rossa in Istria, Croatia. *Geoderma* 91, 125–150. doi:10.1016/S0016-7061(98)00130-X

Durn, G. and Faculty of Mining Geology and Petroleum Engineering, University of Zagreb, Croatia (2003). Terra rossa in the Mediterranean region: Parent materials, composition and origin. *Geol. Croat.* 56/1, 83–100. doi:10.4154/GC.2003.06

Egozcue, J. J., and Pawlowsky-Glahn, V. (2006). "Simplicial geometry for compositional data," in *Compositional data analysis in the geosciences: From theory to practice.* Editors A. Buccianti, G. Mateu-Figueras, and V. Pawlowsky-Glahn (London: Geol. Soc. Spec. Publ.), 264, 145.

Galović, L., and Peh, Z. (2016). Mineralogical discrimination of the Pleistocene loess/paleosol sections in Srijem and Baranja, Croatia. *Aeolian Res.* 21, 151–162. doi:10.1016/j.aeolia.2016.04.006

Grizelj, A., Peh, Z., Tibljaš, D., Kovačić, M., and Kurečić, T. (2017). Mineralogical and geochemical characteristics of Miocene pelitic sedimentary rocks from the south-western part of the Pannonian Basin System (Croatia): Implications for provenance studies. *Geosci. Front.* 8 (1), 65–80. doi:10.1016/j.gsf.2015.11.009

Halamić, J. and Miko, S. (Editors) (2009). *Geochemical atlas of the Republic of Croatia* (Zagreb: Croatian Geological Survey).

Halamić, J., Peh, Z., Miko, S., Galović, L., and Šorša, A. (2012). Geochemical atlas of Croatia: Environmental implications and geodynamical thread. *J. Geochem Explor* 115, 36–46. doi:10.1016/j.gexplo.2012.02.006

Hasan, O., Miko, S., Ilijanić, N., Brunović, D., Dedić, Ž., Šparica Miko, M., et al. (2020). Discrimination of topsoil environments in a karst landscape: An outcome of a geochemical mapping campaign. *Geochem Trans.* 21, 1. doi:10.1186/s12932-019-0065-z

Hinsbergen, D. J. J., Mensink, M., Langereis, C. G., Maffione, M., Spalluto, L., Tropeano, M., et al. (2014). Did Adria rotate relative to Africa? *Solid earth.* 5, 611–629. doi:10.5194/se-5-611-2014

Kelemen, P., Dunkl, I., Csillag, G., Mindszenty, A., Józsa, S., Fodor, L., et al. (2022). Origin, timing and paleogeographic implications of Paleogene karst bauxites in the northern Transdanubian range, Hungary. *Int. J. Earth. Sci.*, 1–22. doi:10.1007/s00531-022-02249-3

Korbar, T. (2009). Orogenic evolution of the external Dinarides in the NE Adriatic region; a model constrained by tectonostratigraphy of Upper Cretaceous to Paleogene carbonates. *Earth-Sci. Rev.* 96, 296–312. doi:10.1016/j.earscirev.2009.07.004

Kovačević Galović, E., Ilijanić, N., Peh, Z., Miko, S., and Hasan, O. (2012). Geochemical discrimination of early Palaeogene bauxites in Croatia. *Geol. Croat.* 65 (1), 53–65. doi:10.4154/GC.2012.04

Kovačić, M., Peh, Z., and Grizelj, A. (2009). Discriminant function analysis of upper Miocene and Pliocene sands from the southwestern part of the Pannonian Basin system, Croatia. *Geol. Croat.* 62 (3), 189–200. doi:10.4154/GC.2009.12

MacLean, W. H., and Barrett, T. J. (1993). Lithogeochemical techniques using immobile elements. *J. Geochem. Explor.* 48, 109–133. doi:10.1016/0375-6742(93)90002-4

Márton, E., Zampieri, D., Grandesso, P., Ćosović, V., and Moro, A. (2010). New Cretaceous paleomagnetic results from the foreland of the Southern Alps and the refined apparent polar wander path for stable Adria. *Tectonophysics* 480, 57–72. doi:10.1016/j.tecto.2009.09.003

Márton, E., Zampieri, D., Kázmér, M., Dunkl, I., and Frisch, W. (2011). New Paleocene–Eocene paleomagnetic results from the foreland of the Southern Alps confirm decoupling of stable Adria from the African plate. *Tectonophysics* 504, 89–99. doi:10.1016/j.tecto.2011.03.006

Merino, E., and Banerjee, A. (2008). Terra rossa genesis, implications for karst, and eolian dust: A geodynamic thread. *J. Geol.* 116, 62–75. doi:10.1086/524675

Mindszenty, A., Csoma, A., Török, Á., Hips, K., and Hertelendi, E. (2000). Flexura jellegű előtéri deformációhoz köthető karsztbauxitszintek a Dunántúli-középhegységben (Rudistid limestones, bauxites, paleokarst and geodynamics. The case of the Cretaceous of the Transdanubian Range). *Bull. Geol. Soc. Hung.* 131, 107–152. (in Hungarian with ext. English abstract).

Mindszenty, A., D'Argenio, B., and Aiello, G. (1995). Lithospheric bulges recorded by regional unconformities. The case of mesozoic-tertiary Apulia. *Tectonophysics* 252, 137–161. doi:10.1016/0040-1951(95)00091-7

Mondillo, N., Balassone, G., Boni, M., Chelle-Michou, C., Cretella, S., Mormone, A., et al. (2019). Rare earth elements (REE) in Al- and Fe-(Oxy)-Hydroxides in bauxites of Provence and Languedoc (southern France): Implications for the potential recovery of REEs as by-products of bauxite mining. *Minerals* 9, 504. doi:10.3390/min9090504

Mondillo, N., Balassone, G., Boni, M., and Rollinson, G. (2011). Karst bauxites in the Campania Apennines (southern Italy): A new approach. *Period. Mineral.* 80, 407–432. doi:10.2451/2011PM0028

Mondillo, N., Nuzzo, M., Kalaitzidis, S., Boni, M., Santoro, L., and Balassone, G. (2022). Petrographic and geochemical features of the B3 bauxite horizon (Cenomanian-Turonian) in the Parnassos-Ghiona area: A contribution towards the genesis of the Greek karst bauxites. *Ore Geol. Rev.* 143, 104759. doi:10.1016/j.oregeorev.2022.104759

Mongelli, G., Boni, M., Buccione, R., and Sinisi, Rosa. (2014). Geochemistry of the Apulian karst bauxites (southern Italy): Chemical fractionation and parental affinities. *Ore Geol. Rev.* 63, 9–21. doi:10.1016/j.oregeorev.2014.04.012

Mongelli, G., Boni, M., Oggiano, G., Mameli, P., Sinisi, R., Buccione, R., et al. (2017). Critical metals distribution in Tethyan karst bauxite: The cretaceous Italian ores. *Ore Geol. Rev.* 86, 526–536. doi:10.1016/j.oregeorev.2017.03.017

Mongelli, G. (2002). Growth of hematite and boehmite in concretions from ancient karst bauxite: Clue for past climate. *Catena* 50, 43–51. doi:10.1016/S0341-8162(02)00067-X

Nesbitt, H. W., and Young, G. M. (1982). Early Proterozoic climates and plate motions inferred from major element chemistry of lutites. *Nature* 299, 715–717. doi:10.1038/299715a0

Nocquet, J.-M. (2012). Present-day kinematics of the mediterranean: A comprehensive overview of GPS results. *Tectonophysics* 579, 220–242. doi:10.1016/j.tecto.2012.03.037

Özlü, N. (1983). Trace element contents of karst bauxites and their parent rocks in the Mediterranean belt. *Min. Deposita* 18 (3), 469–476. doi:10.1007/BF00204491

Papadopoulos, A., Tzifas, I., and Tsikos, H. (2019). The potential for REE and associated critical metals in coastal sand (placer) deposits of Greece: A review. *Minerals* 9, 469. doi:10.3390/min9080469

Pawlowsky-Glahn, V., Egozcue, J. J., and Tolosana-Delgado, R. (2007). Lecture notes on compositional data analysis. Available at: https://www.researchgate.net/publication/37814008_Lecture_Notes_on_Compositional_Data_Analysis (Accessed November 20, 2022).

Peh, Z., and Halamić, J. (2010). Discriminant function model as a tool for classification of stratigraphically undefined radiolarian cherts in ophiolite zones. *J. Geochem. Explor.* 107, 30–38. doi:10.1016/j.gexplo.2010.06.003

Peh, Z., and Kovačević Galović, E. (2014). Geochemistry of Istrian Lower Palaeogene bauxites – is it relevant to the extent of subaerial exposure during Cretaceous times? *Ore Geol. Rev.* 63, 296–306. doi:10.1016/j.oregeorev.2014.05.020

Peh, Z., and Kovačević Galović, E. (2016). Geochemistry of Lower Palaeogene bauxites – unique signature of the tectonostratigraphic evolution of a part of the Croatian Karst. *Geol. Croat.* 69 (2), 269–279. doi:10.4154/gc.2016.24

Peh, Z., Šajn, R., Halamić, J., and Galović, L. (2008). Multiple discriminant analysis of the Drava River alluvial plain sediments. *Environ. Geol.* 55, 1519–1535. doi:10.1007/s00254-007-1102-2

Putzolu, F., Papa, A., Mondillo, N., Boni, M., Balassone, G., and Mormone, A. (2018). Geochemical characterization of bauxite deposits from the Abruzzi mining district (Italy). *Minerals* 8, 298. doi:10.3390/min8070298

Radusinović, S., Jelenkovic, R., Pačevski, A., Simić, V., Božović, D., Holclajtner-Antunović, I., et al. (2016). Content and mode of occurrences of rare earth elements in the Zagrad karstic bauxite deposit (Nikšić area, Montenegro). *Ore Geol. Rev.* 80, 406–428. doi:10.1016/j.oregeorev.2016.05.026

Radusinović, S., and Papadopoulos, A. (2021). The potential for REE and associated critical metals in karstic bauxites and bauxite residue of Montenegro. *Minerals* 11, 975. doi:10.3390/min11090975

Razum, I., Bajo, P., Brunović, D., Ilijanić, N., Hasan, O., Röhl, U., et al. (2021). Past climate variations recorded in needle-like aragonites correlate with organic carbon burial efficiency as revealed by lake sediments in Croatia. *Sci. Rep.* 11, 7568. doi:10.1038/s41598-021-87166-2

Razum, I., Miko, S., Ilijanić, N., Hasan, O., Šparica Miko, M., Brunović, D., et al. (2020a). A compositional approach to the reconstruction of geochemical processes involved in the evolution of Holocene marine flooded coastal karst basins (Mljet Island, Croatia). *Appl. Geochem.* 116, 104574. doi:10.1016/j.apgeochem.2020.104574

Razum, I., Miko, S., Ilijanić, N., Petrelli, M., Röhl, U., Hasan, O., et al. (2020b). Holocene tephra record of Lake Veliko jezero, Croatia: Implications for the central mediterranean tephrostratigraphy and sea level rise. *Boreas* 49 (3), 653–673. doi:10.1111/bor.12446

Reimann, C., Filzmoser, P., Fabian, K., Hron, K., Birke, M., Demetriades, A., et al. (2012). The concept of compositional data analysis in practice – total major element concentrations in agricultural and grazing land soils of Europe. *Sci. Total. Environ.* 426, 196–210. doi:10.1016/j.scitotenv.2012.02.032

Reimann, C., Filzmoser, P., Garrett, R. G., and Dutter, R. (2008). *Statistical data analysis explained: Applied environmental statistics with R*. New York: John Wiley & Sons.

Rock, N. M. S. (1988). *Lecture notes in earth Sciences, 18: Numerical Geology*. Berlin: Springer-Verlag.

Rudnick, R., and Gao, S. (2013). Composition of the continental crust. *Treatise Geochem.* 3, 1–51. doi:10.1016/B978-0-08-095975-7.00301-6

Sakač, K., and Šinkovec, B. (1991). The bauxites of the Dinarides. *Trav. ICSOBA* 21, 1–11.

Schmid, S., Fügenschuh, B., Kounov, A., Matenco, L., Nievergelt, P., Oberhänsli, R., et al. (2020). Tectonic units of the Alpine collision zone between Eastern Alps and western Turkey. *Gondwana Res.* 78, 308–374. doi:10.1016/j.gr.2019.07.005

Schmid, S. M., Bernoulli, D., Fügenschuh, B., Matenco, L., Schefer, S., Schuster, R., et al. (2008). The Alpine-Carpathian-Dinaridic orogenic system: Correlation and evolution of tectonic units. *Swiss J. Geosci.* 101, 139–183. doi:10.1007/s00015-008-1247-3

Scisciani, V., and Calamita, F. (2009). Active intraplate deformation within Adria: Examples from the Adriatic region. *Tectonophysics* 476, 57–72. doi:10.1016/j.tecto.2008.10.030

Sinisi, R. (2018). Mineralogical and geochemical features of Cretaceous bauxite from San Giovanni Rotondo (Apulia, southern Italy): A provenance tool. *Minerals* 8, 567. doi:10.3390/min8120567

Šinkovec, B., and Sakač, K. (1991). Bauxite deposits of Yugoslavia — The state of the art. *Acta Geol. hung.* 34/4, 307–315.

Šinkovec, B., and Sakač, K. (1982). The Paleogene bauxites of Dalmatia. *Trav. ICSOBA* 12, 293–331.

Šinkovec, B., Šušnjara, A., and Sakač, K. (1985). Boksiti Korduna i susjednih područja. *Geol. Vjesn.* 38, 215–233.

Šorša, A., Peh, Z., and Halamić, J. (2018). Geochemical mapping the urban and industrial legacy of Sisak, Croatia, using discriminant function analysis of topsoil chemical data. *J. Geochem. Explor.* 187, 155–167. doi:10.1016/j.gexplo.2017.07.014

StatSoft, Inc. (2006). STATISTICA (data analysis software system). Available at: www.statsoft.com2006.

Šumanovac, F. (2010). Lithosphere structure at the contact of the Adriatic microplate and the Pannonian segment based on the gravity modelling. *Tectonophysics* 485, 94–106. doi:10.1016/j.tecto.2009.12.005

Šušteršič, F., Rejšek, K., Mišič, M., and Eichler, F. (2009). The role of loamy sediment (terra rossa) in the context of steady state karst surface lowering. *Geomorphology* 106, 35–45. doi:10.1016/j.geomorph.2008.09.024

Tarvainen, T., Reeder, S., and Albanese, S. (2005). "Database management and map production," in *Geochemical atlas of Europe, Part 1, background information, methodology and Maps*. Editors R. Salminen, M. J. Batista, M. Bidovec, A. Demetriades, B. De Vivo, W. De Vos, et al. (Geological Survey of Finland, Espoo).

Thiffault, E. (2019). "Boreal forests and soils," in *Developments in soil science 36 global change and forest soils*. Editors M. Busse, C. P. Giardina, D. M. Morris, and D. S. Page-Dumroese (Amsterdam: Elsevier), 59–82. doi:10.1016/B978-0-444-63998-1.00005-7

Tolosana-Delgado, R., Otero, N., and Pawlowsky-Glahn, V. (2005). Some basic concepts of compositional geometry. *Math. Geol.* 37, 673–680. doi:10.1007/s11004-005-7374-8

Tolosana-Delgado, R. (2012). Uses and misuses of compositional data in sedimentology. *Sediment. Geol.* 280, 60–79. doi:10.1016/j.sedgeo.2012.05.005

Tomašić, N., Čobić, A., Bedeković, M., Miko, S., Ilijanić, N., Gizdavec, N., et al. (2021). Rare earth elements enrichment in the upper Eocene Tošići-Dujići bauxite deposit, Croatia, and relation to REE mineralogy, parent material and weathering pattern. *Minerals* 11, 1260. doi:10.3390/min11111260

Ustaszewski, K., Kounov, A., Schmid, S., Schaltegger, U., Krenn, E., Frank, W., et al. (2010). Evolution of the Adria-Europe plate boundary in the northern

Dinarides: From continent-continent collision to back-arc extension. *Tectonics* 29. doi:10.1029/2010TC002668

Valeton, I., Biermann, M., Reche, R., and Rosenberg, F. (1987). Genesis of nickel laterites and bauxites in Greece during the Jurassic and Cretaceous, and their relation to ultrabasic parent rocks. *Ore Geol. Rev.* 2, 359–404. doi:10.1016/0169-1368(87)90011-4

van Breemen, N., and Buurman, P. (1998). *Ferralitization in soil formation*. Wagenigen, The Netherlands: Kluwer Academic Publishers, 291–312.

Vlahović, I., Tišljar, J., Velić, I., and Matičec, D. (2005). Evolution of the Adriatic carbonate platform: Palaeogeography, main events and depositional dynamics. *Palaeogeogr. Palaeoclimat. Palaeoecol.* 220, 333–360. doi:10.1016/j.palaeo.2005.01.011

Vlahović, I., Tišljar, J., Velić, I., Matičec, D., and Maticec, D. (2002). The karst Dinarides are composed of relics of a single Mesozoic platform: Facts and consequences. *Geol. Croat.* 55/2, 171–183. doi:10.4154/GC.2002.15

Weaver, C. E. (1989). *Clays, muds, and shales*. Amsterdam: Elsevier.

Yang, S., Qingfei, W., Deng, J., Wang, Y., Kang, W., Liu, X., et al. (2019). Genesis of karst bauxite-bearing sequences in Baofeng, Henan (China), and the distribution of critical metals. *Ore Geol. Rev.* 115, 103161. doi:10.1016/j.oregeorev.2019.103161

Zhao, L., Liu, X., Yang, S., Ma, X., Liu, L., and Sun, X. (2021). Regional multi-sources of Carboniferous karstic bauxite deposits in North China Craton: Insights from multi-proxy provenance systems. *Sediment. Geol.* 421, 105958. doi:10.1016/j.sedgeo.2021.105958